Supplementary Information

In-situ Cadmium Surface Passivation of Perovskite Nanocrystals for Blue LEDs

Woo Hyeon Jeong[a,‡], Zhongkai Yu[b,‡], Luca Gregori[c,‡], Jonghee Yang[a,d,‡], Su Ryong Ha[a], Ji Won Jang[a], Hochan Song[a], Jong Hyun Park[e], Eui Dae Jung[e,f], Myoung Hoon Song[e], Sung Heum Park[b], Henry J. Snaith[g], Alberto Boretti[h], Filippo De Angelis[c,i], Daniele Meggiolaro[j,*], Jeongjae Lee[k,*], Hyosung Choi[a,*], and Bo Ram Lee[b,*]

[a]Department of Chemistry, Research Institute for Convergence of Basic Science, and Research Institute for Natural Sciences, Hanyang University, Seoul 04763, Republic of Korea, hschoi202@hanyang.ac.kr

[b]Department of Physics, Pukyong National University Busan 48513, Republic of Korea
E-mail: brlee@pknu.ac.kr

[c]Department of Chemistry, Biology and Biotechnology, University of Perugia, Perugia, Italy.

[d]Institute for Advanced Materials and Manufacturing, Department of Materials Science and Engineering, University of Tennessee, Knoxville, TN 37996, USA

[e]Department of Materials Science and Engineering, Ulsan National Institute of Science and Technology (UNIST) Ulsan 44919, Republic of Korea

[f]Department of Electrical and Computer Engineering, University of Toronto, 10 King's College Road, Toronto, Ontario M5S 3G4, Canada

[g]Clarendon Laboratory, Department of Physics, University of Oxford, Oxford, UK.

[h]Department of Mechanical Engineering, College of Engineering, Prince Mohammad Bin Fahd University, P.O. Box 1664 Al Khobar 31952, Kingdom of Saudi Arabia.

[i]Department of Natural Sciences & Mathematics, College of Sciences & Human Studies, Prince Mohammad Bin Fahd University, P.O. Box 1664 Al Khobar 31952, Kingdom of Saudi Arabia.

[j]Computational Laboratory for Hybrid/Organic Photovoltaics (CLHYO), Istituto CNR di Scienze e Tecnologie Chimiche 'Giulio Natta' (CNR-SCITEC), Perugia, Italy.
E-mail: daniele.meggiolaro@cnr.it

[k]School of Earth and Environmental Sciences, Seoul National University Seoul 08826, Republic of Korea
E-mail: jl635@snu.ac.kr

‡These authors contributed equally: Woo Hyeon Jeong, Zhongkai Yu, Luca Gregori, Jonghee Yang.

Contents:

1. Experimental section

1.1 Materials

Cesium carbonate (99.9%), Cadmium chloride ($CdCl_2$; technical grade), (1-octadecene (ODE, 90% tech.), oleylamine (OLA, 70% tech.), Oleic acid (OA, 90% tech.), Methylacetate (MeOAc; anhydrous 99.5%), Octane (anhydrous, ≥99%), Toluene (anhydrous 99.8%), Trioctylphosphine (TOP; 97%), Hexane (anhydrous 95%), Chlorobenzene (99.8%), and Didodecyldimethylammonium bromide (DDAB 98%) were purchased from Sigma Aldrich. Lead bromide ($PbBr_2$; 99.999%) and Lead chloride ($PbCl_2$; 99.999%) were purchased form Alfa Aesar. Indium tin oxide-based transparent conductive electrode (~4.5 Ω/sq) purchased from AMG. Aqueous solution of PEDOT:PSS (Clevios AI 4083) purchased from Heraeus. Poly[bis(4-phenyl) (4-butylphenyl) amine] (poly-TPD) and 2,2′,2″-(1,3,5-benzinetriyl)tris(1-phenyl-1-H-benzimidazole) (TPBi; 99.9%) were purchased from OSM. LiF (99.9%) and Al (99.9%) were purchased form iTASCO.

1.2 Preparation of the nanocrystals

Cesium-oleate solution: Cs_2CO_3 (0.407g), 1.25ml of pre-degassed OA and 20ml ODE were put into 100ml 3-neck flask and degassed under vacuum at 120 °C for 1h. After degassing, N_2 gas was filled into flask and then the temperature was increased to 140 °C.

$CsPbBr_2Cl$ NCs synthesis: $PbBr_2$ (0.265g), $PbCl_2$ (0.1g), 2.5ml pre-degassed OA, 2.5ml pre-degassed OLA, 2.5ml TOP and 25ml ODE were put into 100ml 3-neck flask and degassed under vacuum at 120 °C for 1h. After degassing, N_2 gas was filled into flask and then the temperature was increased to 180 °C. When the temperature reaches 180 °C, Cesium-oleate solution (2ml) was swiftly injected into flask. After 10 second, heating mantle was removed and cooling the flask with ice bath.

Cd-$CsPbBr_2Cl$ NCs synthesis: Cd concentration was tuned by changing the ratio of $PbCl_2$ and $CdCl_2$. Cd 0.2% NCs was $PbBr_2$ (0.265g), $PbCl_2$ (0.085g) and $CdCl_2$ (0.01g). Cd 0.4% NCs was $PbBr_2$ (0.265g), $PbCl_2$ (0.07g) and $CdCl_2$ (0.02g). Cd 0.8% was $PbBr_2$ (0.265g), $PbCl_2$ (0.04g) and $CdCl_2$ (0.04g). All the other parameters were kept unchanged.

Purification: 15ml of crude solution and 35ml of MeOAc as an anti-solvent, were mixed and centrifuged 8,000rpm for 5min. After that, supernatant was discarded. Dispersing the remaining NCs in 5ml of hexane, 8ml of MeOAc was added in NCs solution and centrifuged at 8,000rpm for 5min. The purified NCs was dispersed in 5ml hexane and filtered with 0.2μm PTFE syringe filter (Whatman) and stored.

Ligand exchange: Purified OA and OLA capped NCs are dispersed in toluene (8mg ml^{-1}). OA (100 μL) and 0.05M DDAB solution (23.1mg ml^{-1} in toluene) 200 μL are added into NCs solution and stirring 30min. For purification, 2ml MeOAc was added in exchanged NCs solution 1ml, and centrifuged at 8000rpm for 5min. The NCs were dispersed in octane (5mg ml^{-1}) for LED fabrication.

1.3 Device fabrication

For PeLED devices, a conventional device structure consisting of indium tin oxide (ITO) as anode, poly(ethylenedioxythiophene):polystyrene sulfonate (PEDOT:PSS) and poly[bis(4-phenyl) (4-butylphenyl) amine] (poly-TPD) as hole transport layer (HTL), Cd-PNCs as emissive layer, 2,2′,2″-(1,3,5-benzinetriyl)tris(1-phenyl-1-H-benzimidazole) (TPBi) as electron transport layer (ETL) and exciton blocking layer (EBL), lithium fluoride (LiF) as electron injection layer (EIL) and aluminum (Al) as cathode; ITO/PEDOT:PSS/poly-TPD/Cd-PNCs/TPBi/LiF/Al. ITO was washed by ultrasonic treatment in deionized water (DI water), acetone, and 2-propanol for 10 min each. After drying in an oven, the ITO substrates were treated with O_2 plasma for 10 min. The PEDOT:PSS(AI 4083) solution was spin coated on ITO at 4,500 rpm for 40 seconds and annealed at 140 °C on the hotplate for 10 min. The substrates were transferred into glove box. Poly-TPD (in chlorobenzene10mg ml^{-1}) layer was spin coated on PEDOT:PSS layer at 4,000rpm for 40 seconds and annealed at 120°C on the hotplate for 5 min. After annealed, perovskite nanocrystal (in octane 5mg ml^{-1}) emissive layer was spin coated on poly-TPD layer at 2,000 rpm for 20 seconds. Finally, TPBi (60 nm), LiF (1 nm), and Al (100 nm) were sequentially deposited at ~10^{-6} Torr by the thermal evaporation method. The area of the Al electrode defines a 0.135 cm^2 emission area of the device.

1.4 Ab initio calculations

DFT calculations have been performed at the Γ- point by using the CP2K code[1]. The Perdew-Burke-Ernzerhof (PBE) functional[2] with DFT-D3 van der Waals correction[3], norm-conserving Goedecker-Teter-Hutter pseudopotentials[4] and TZVP Gaussian basis set[5] have been used

along with a density cutoff of 300 Ry on the charge density.

In order to build the mixed $CsPbBr_2Cl$ phase, we monitored the energies of two configurations with 2 Cl ions substituting Br in the $[PbBr_6]^{2-}$ octahedra in the 3D $CsPbBr_3$ bulk phase: i) two equatorial Cl; ii) Cl ions placed in equatorial and axial positions. In both cases the cell has been relaxed to find the optimal cell parameters. Configuration ii) is more stable than i) by 0.08 eV and it has been used to build slab models for surface calculations. The energy of substitution of Br by Cl in $CsPbBr_3$ 3D bulk phase has been calculated by considering halide exchange between Br_2 / Cl_2 molecules and the perovskite and it is favored by 0.23 eV. The energy of Pb substitution by Cd has been calculated by simulating metal exchange between $PbCl_2$ / $CdCl_2$ phases and the pristine perovskite.

Surface calculations have been performed in the 2x2 in-plane slab models, by fixing cell parameters to the optimized values calculated in the bulk and adding 15 Å of vacuum along the non-periodic direction perpendicular to the surface.

Surface formation energies have been calculated starting from the $PbBr_2$, CsBr, $CdBr_2$ phases for $CsPbBr_3$ pristine and Cd-doped surfaces and from $PbBr_2$, $PbCl_2$, CsBr, $CdCl_2$ for the $CsPbBr_2Cl$ pristine and Cd-doped surfaces, by using the expression

$$SFE = \frac{E^s - \sum n_i \mu_i}{2A} \qquad \text{(eq 1)}$$

where E^s represent the energy of the modelled slab, n_i are the numbers of $PbBr_2$, CsBr, $PbCl_2$, $CdCl_2$, $CdBr_2$ units composing the slabs and μ_i are the energies of the relative phases; A is the slab surface area. Work function (WF) has been calculated as the difference between the potential in the vacuum and the VBM of the slab.

1.5 Characterization

SEM were measured with Verios G4 UC (FEI) Smart Lab at the Hanyang LINC + analytical equipment center (Seoul). with beam energy of 5kV (cross-sectional) and 15 kV (element mapping). XPS spectra were collected using an angle-resolved photoelectron spectrometer (Thermo Fisher Scientific, Theta Probe) at the Hanyang LINC + analytical equipment center (Seoul). A sample-to-detector take-off angle of 30° with respect to surface normal was employed to selectively obtain surface-oriented signals while excluding bulk-oriented signals.

For surface etching, Ar^+ plasma (1 keV, 1 μA) was bombarded onto the PNC surface for 2 to 5 s within the XPS chamber, where the selective elimination of the uppermost surface species were monitored by the disappearance of N 1s photoelectron signal oriented from surface-binding OLA. PLQY measurement of the perovskite NCs solution dispersed in hexane was conducted with a QE-2000 (Otsuka Photal Electronics) equipped with an integrating hemisphere, and samples were excited at the wavelength of 365 nm. UV-Vis absorption spectra were measured on a Varian Cary 5000 spectrophotometer. Steady-state PL measurements were carried out using a pulsed xenon lamp. And time-resolved PL decay measurements were carried out using a He-Cd laser operating at a wavelength of 375 nm. For PeLEDs, J-V-L characteristics and device performances were measured using a Konica Minolta spectroradiometer (CS- 2000) with a Keithley 2400 source meter. PeLED device characteristics were measured under ambient air conditions without any encapsulation. XRD patterns were measured using a using an X'Pert-MPD diffractometer (Philips, Netherlands) employing CuKα radiation. TEM samples were prepared by diluted NC solution in hexane dropped on an ultrathin carbon film grid. TEM were measured with JEM-2100F model (JEOL). Solid-state NMR spectra were measured at 11.75 T (National Center for Inter-University Research Facilities, Seoul National University) with 4 mm Bruker Magic-Angle Spinning (MAS) probe. PNC samples were packed into Kel-F inserts and were spun at 5 kHz. ^{133}Cs spectra were referenced to solid CsBr (260.3 ppm). Recycle delays of 20 s were used for all samples. The Fourier transform infrared (FT-IR) was recorded on PerkinElmer Spectrum Two FT-IR Spectrometer.

Supplementary Note 1. Discrepancy in Cd detection between XPS and EDS techniques

XPS is a surface-sensitive technique, with a confined information (electron escape) depth of ~10 nm, and exclusively detects surface-oriented signals. Thus, XPS measurement can in theory be regarded as a suitable analytic tool to confirm the presence and binding nature of surface Cd contents. However, detection of a relatively light element (Cd Z=48) in a matrix of heavy elements (e.g., Pb Z=82) is normally deemed difficult due to the large photoemission intensities of heavy elements (which in general scales with Z). Moreover, the overlapping emission lines of Cd with Pb/Br (e.g., Cd $3d_{3/2}$ and Pb$4d_{5/2}$ both ~412 eV) makes the detection of low-level Cd difficult; a previous comprehensive study of XPS sensitivities estimate this lower limit of detection to be around 0.3 to 1%, which puts our estimated Cd content (0.2~0.8% with respect to Pb) on the borderline of detection limit[6].

The situation, however, becomes more favorable for EDS (elemental mapping) collected from an SEM instrument, since the initial excitation comes from the relatively high-energy electrons (5-20 keV) with respect to that of XPS (Al Kα~1488 eV), which subsequently results in larger interaction volumes and deeper information depth (roughly >100 nm). Moreover, the characteristic X-ray emission coming from Cd now has kinetic energies order of magnitude larger than the photoemission (Cd Lα=3.1 keV vs Cd $3d_{5/2}$=1488–405=1083 eV), which would make detection in EDS more favorable.

Supplementary Note 2. Surface Cl upon Cd incorporation

It is also noteworthy that the Cl/Br ratio gradually increases as PNC becomes Cd-rich, likely as a consequence of extra Cl incorporation from $CdCl_2$, but dramatically reduced and reached to the nominal bulk level (closer to halide ratios of neat PNC) upon surface etching (Figure S10). This implies that the extra Cl species must be preferentially located at the surface of PNCs rather than in the bulk, consistent with the observation of negligible PL shift for the low-Cd PNCs (i.e., the bulk halide composition was retained). Indeed, the Cl 2p spectra of both Cd-bulk and Cd-surface PNCs, upon surface etching, revealed the coexistence of surface and bulk Cl components (Figure S11)[7]. Note that the surface/bulk Cl ratio of the PNCs, obtained from the Cl 2p spectra, are similar to each other (Table S5). These observations collectively suggest that the extra surface Cl species may contribute to stabilizing the surface Cd^{2+}. This surface Cl species could further suppress the halide vacancies at the PNC surface by filling the vacant sites in the vicinity of them without compromising the optical characteristics[8,9].

Supplementary Note 3. Device operational stabilites

To further investigate the device stability of PeLEDs, we measured the long-term device stability under a constant voltage of 3.2 V. The time to 50% of initial luminance (T_{50}) in optimized device is 140 seconds, which is 2.5 times longer than that of the reference device (56 seconds), as shown in **Figure S19**a,b. In addition, stable blue emission along with whole lifetime is observed with identical EL spectra at T_{25}, T_{50} and T_{75}. (See **Figure S19**c,d), which signifies an effective suppression of halide segregation as a result of combined surface engineering through Cd^{2+} doping and DDAB passivation.

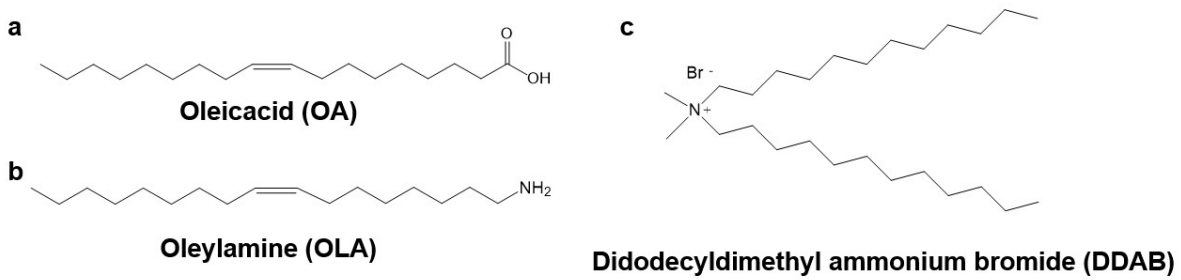

Figure S1. Chemical structure of a) Oleic acid, b) Oleylamine and c) Didodecyldimethylammonium bromide.

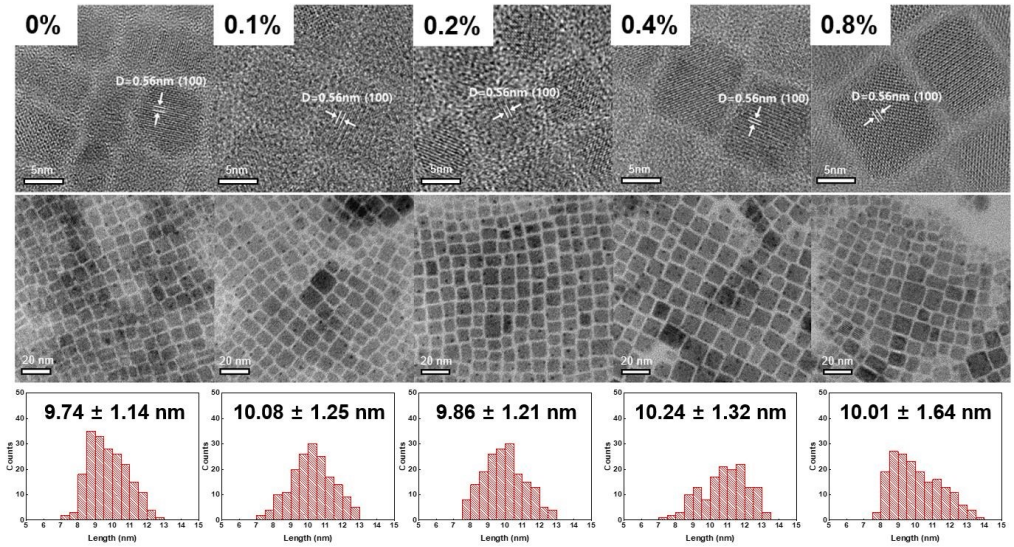

Figure S2. High resolution transmission electron microscopy images of Cd-$CsPbBr_2Cl$ PNCs after the capping with DDAB ligand and size histogram.

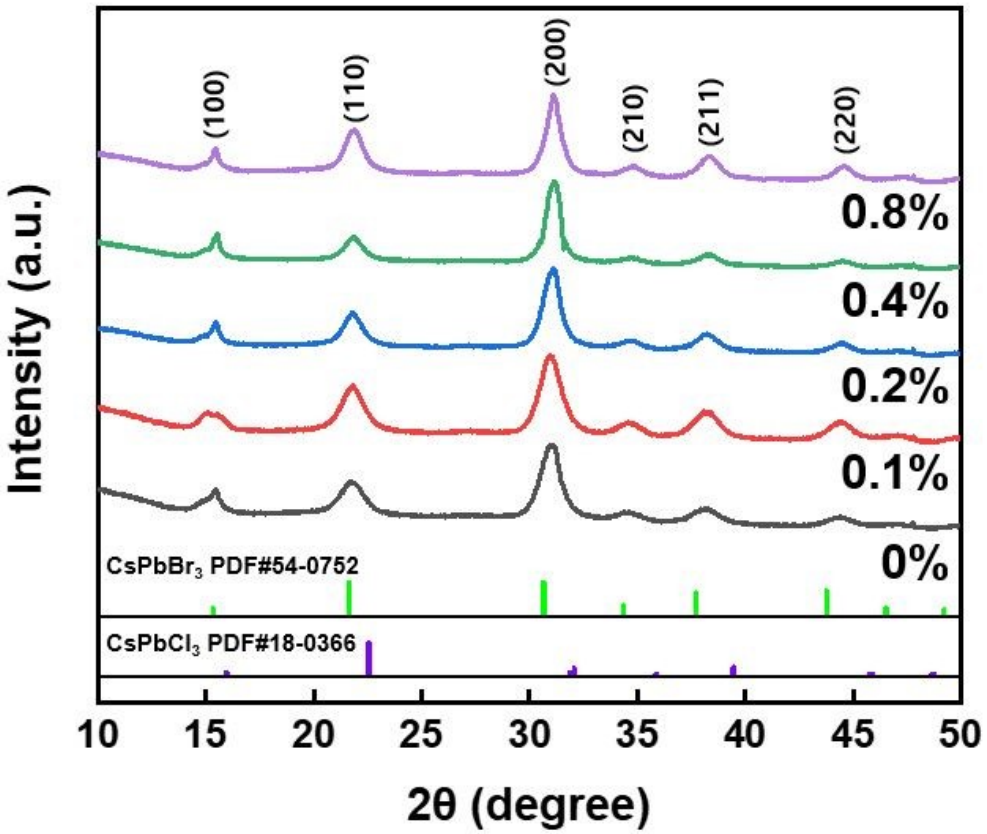

Figure S3. Powder X-ray diffraction pattern for Cd-doped PNCs.

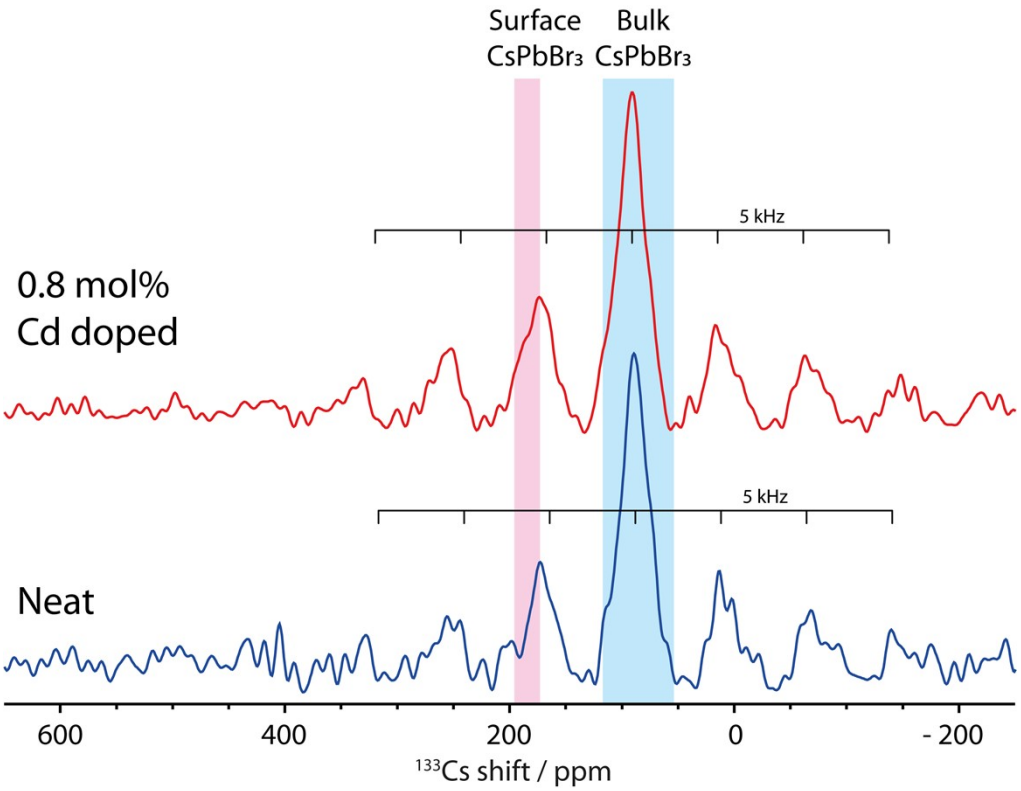

Figure S4. ^{133}Cs solid-state NMR spectra for 0.8 mol% Cd-doped and neat PNCs. Locations of expected spinning sidebands (5 kHz MAS) are indicated.

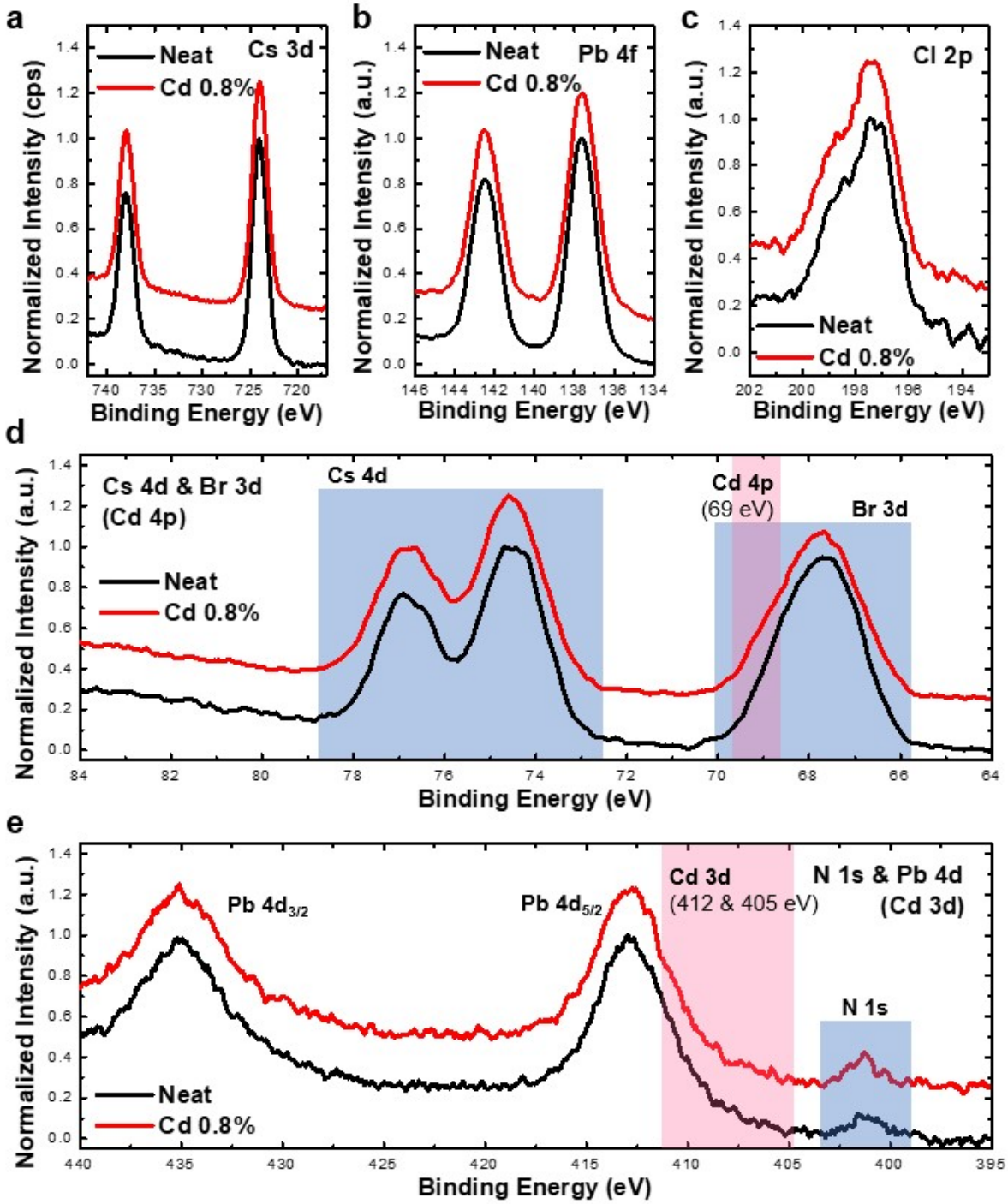

Figure S5. XPS spectra of 0.8 mol% Cd-doped and neat PNCs. a) Cs 3d, b) Pb 4f, c) Cl 2p d) Cs 4d, Br 3d and Cd 4p, e) Pb $4d_{3/2}$ Pb $4d_{5/2}$ Cd 3d, N 1s, Pb 4d and Cd 3d.

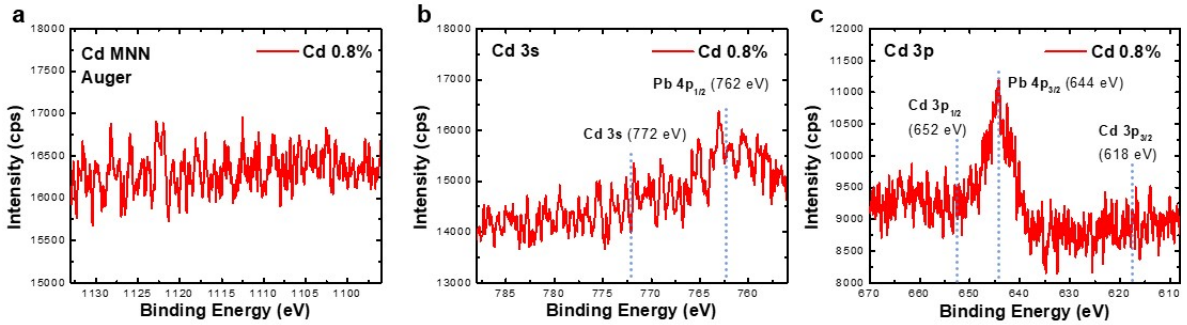

Figure S6. XPS Cd spectrums of 0.8 mol% Cd-doped PNCs. No Cd was detected.

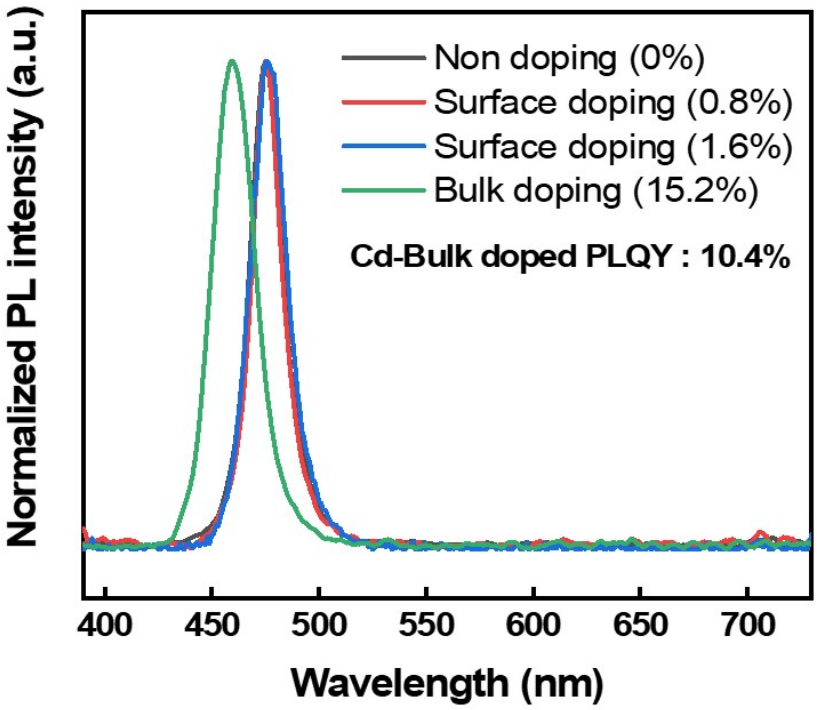

Figure S7. Photoluminescence spectra of surface- and bulk-doped Cd-PNCs.

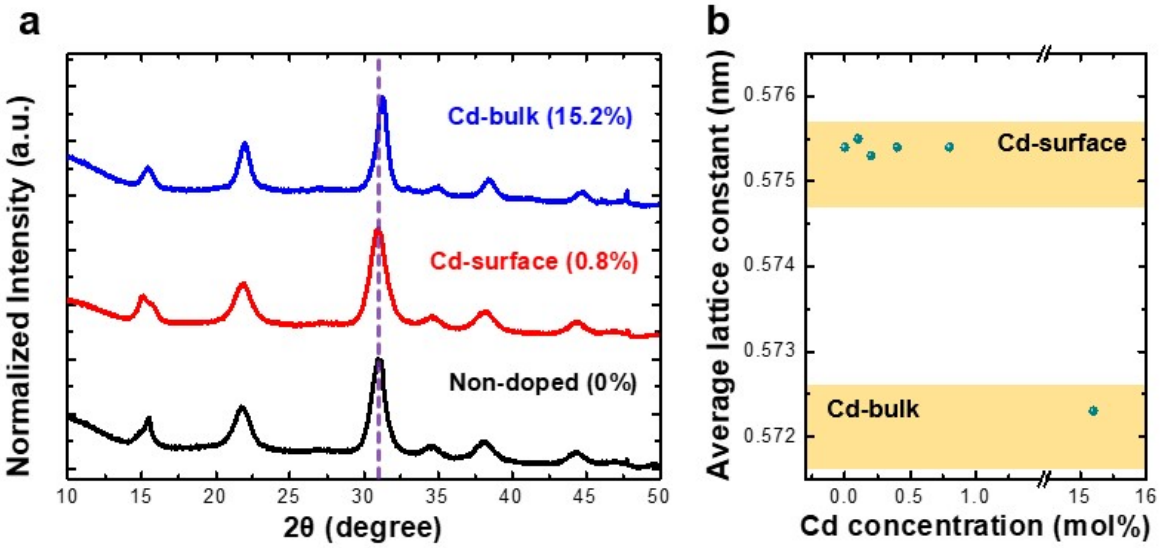

Figure S8. a) PXRD patterns of neat (non-doped), Cd-surface (0.8%) and Cd-bulk (15.2%)PNCs. b) Estimated average lattice constant of the PNCs demonstrated in this study.

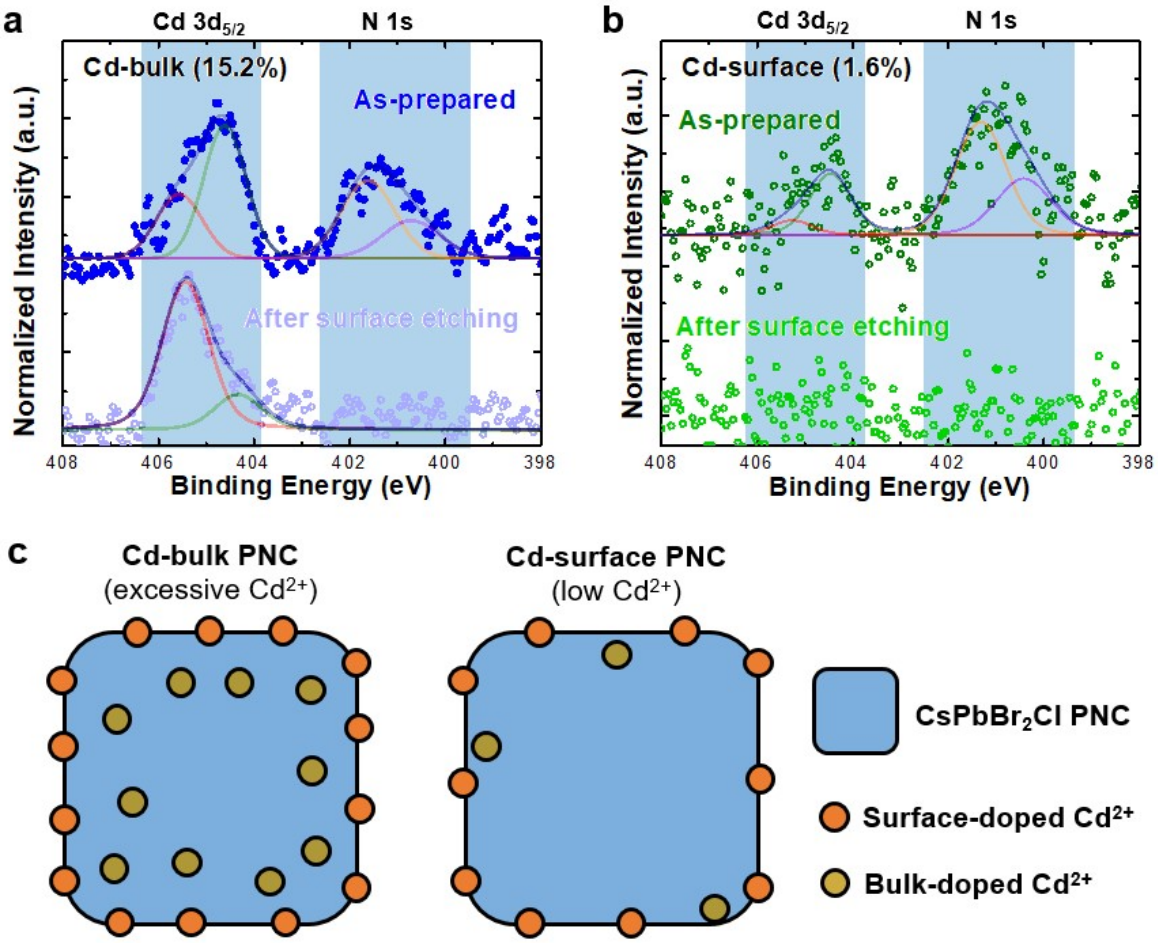

Figure S9. Cd 3d (and N 1s) core-level XPS spectra of a) Cd-bulk (15.2%) and b) Cd-surface (1.6%) PNCs before and after surface etching. c) Schematics describing Cd-bulk (left) and Cd-surface (right) PNCs.

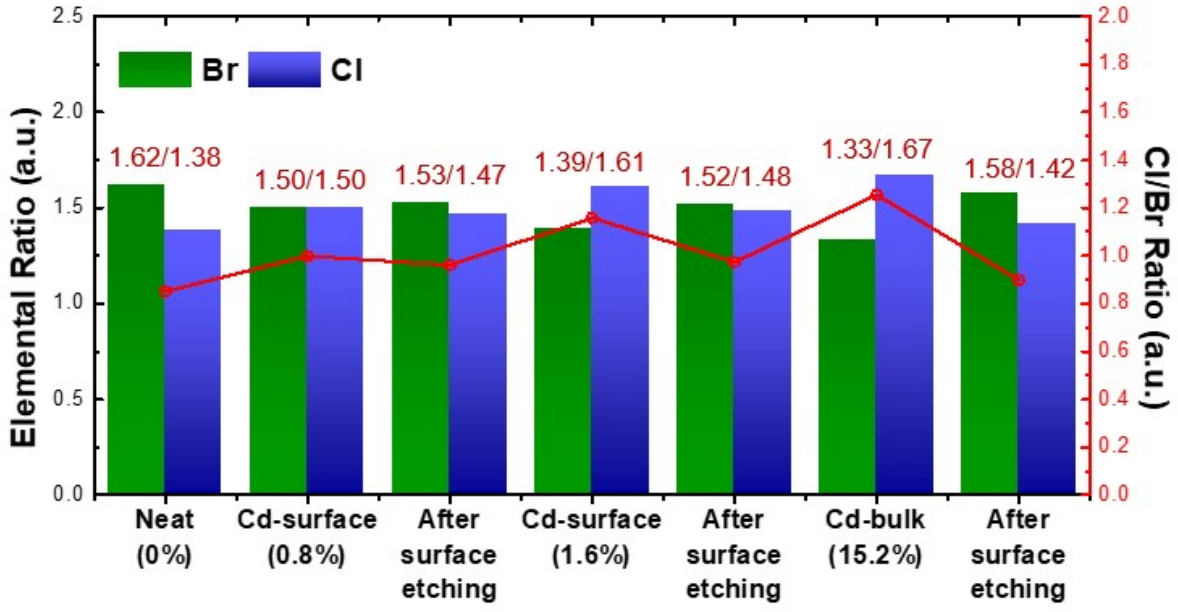

Figure S10. Estimated halide composition ratios of the PNCs based on the XPS analysis. Relative Br/Cl ratios (assuming balanced stoichiometry) of each condition are labeled

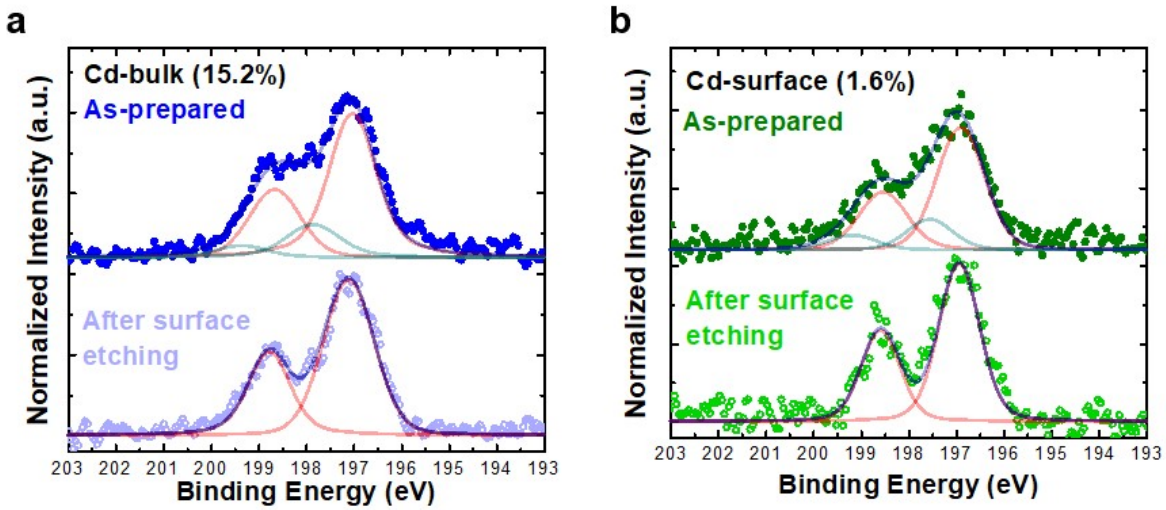

Figure S11. Cl 2p core-level XPS spectra of a) Cd-bulk (15.2%) and b) Cd-surface (1.6%) PNCs before and after surface etching.

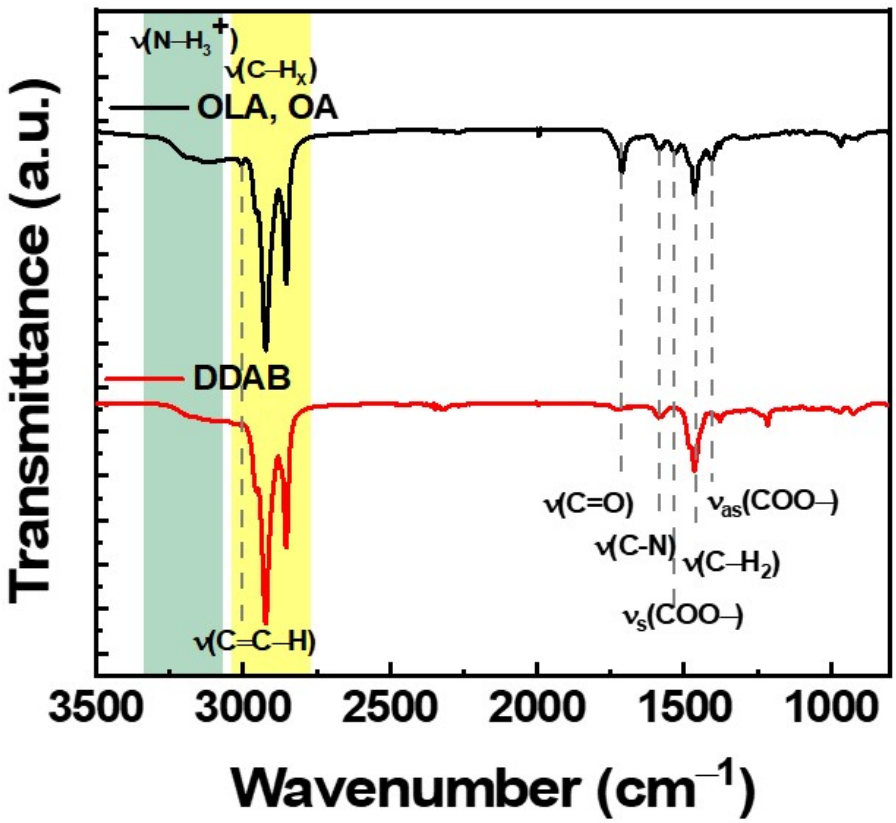

Figure S12. FT-IR spectra for PNCs with OA/OLA encapsulation (black trace) and DDAB encapsulation (red trace). Frequencies for expected functional groups in OA/OLA/DDAB are indicated.

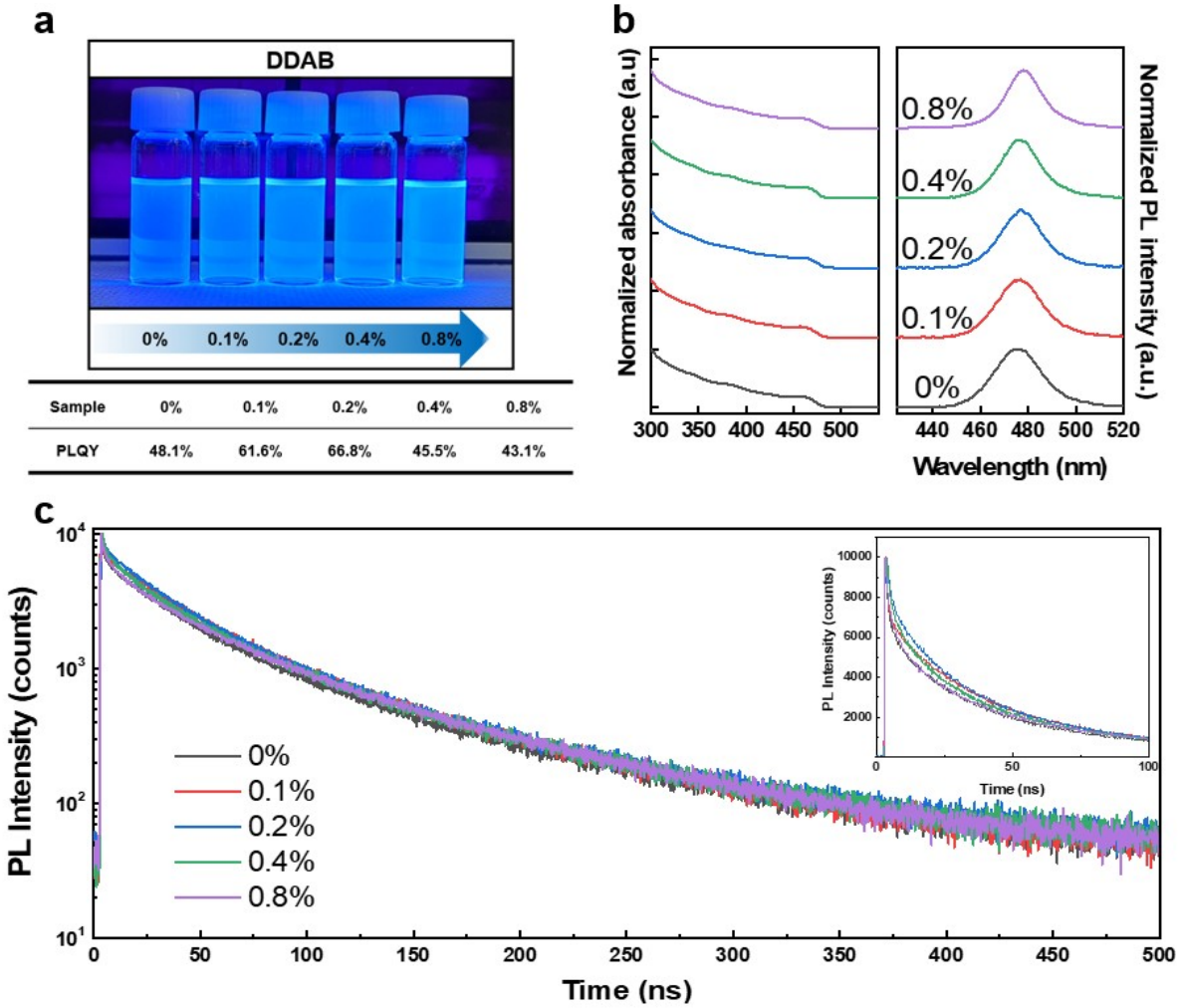

Figure S13. Optical properties of Cd-PNCs after ligand exchange with DDAB. a) Photographic images of perovskite NCs solutions under 365 nm UV lamp illumination and photoluminescence quantum yield table. b) Normalized absorption and PL spectra of the PNC dispersions. c) PL decay curves of DDAB-exchanged PNCs as increasing Cd concentrations. An inset clearly reveals that the faster decay component was gradually alleviated upon Cd doping upto 0.2%, suppressing non-radiative recombination.

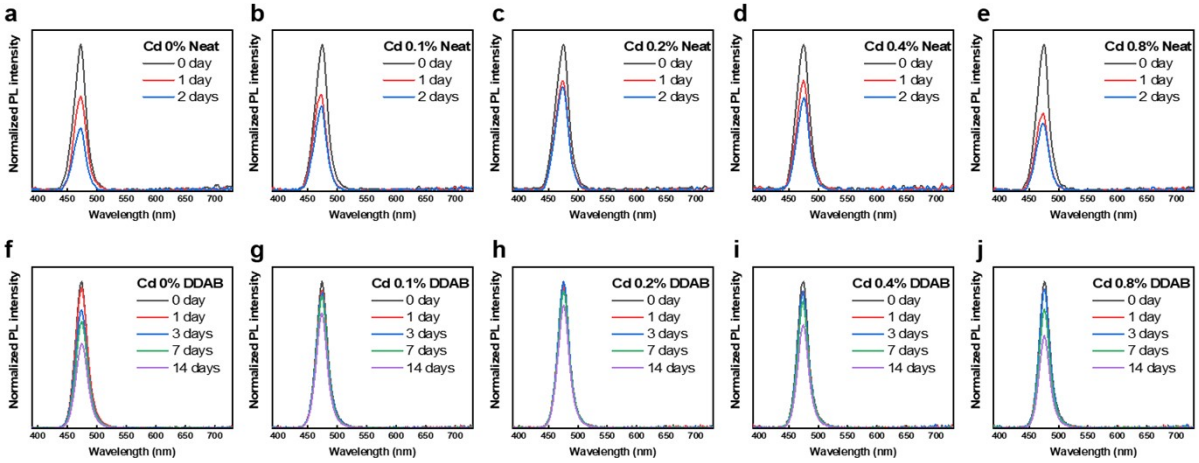

Figure S14. Storage time-dependent PL spectra of a-e) Neat PNCs and f-j) DDAB PNCs in ambient condition.

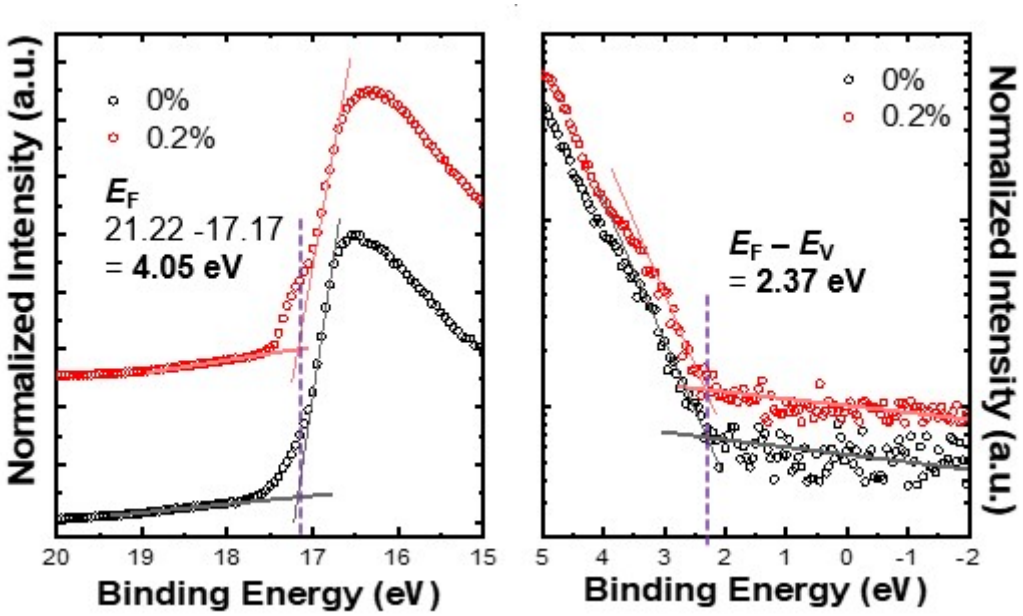

Figure S15. UPS spectra of Cd-0% and 0.2% Cd-PNCs.

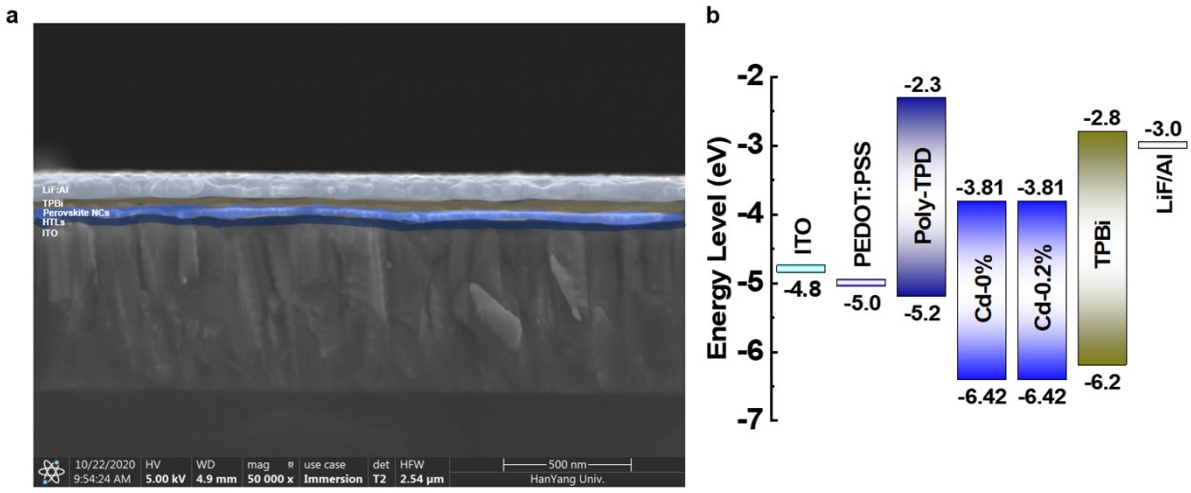

Figure S16. Cross-sectional scanning electron microscopy image of the prepared PeLED device. b) Energy level diagram of PeLED device.

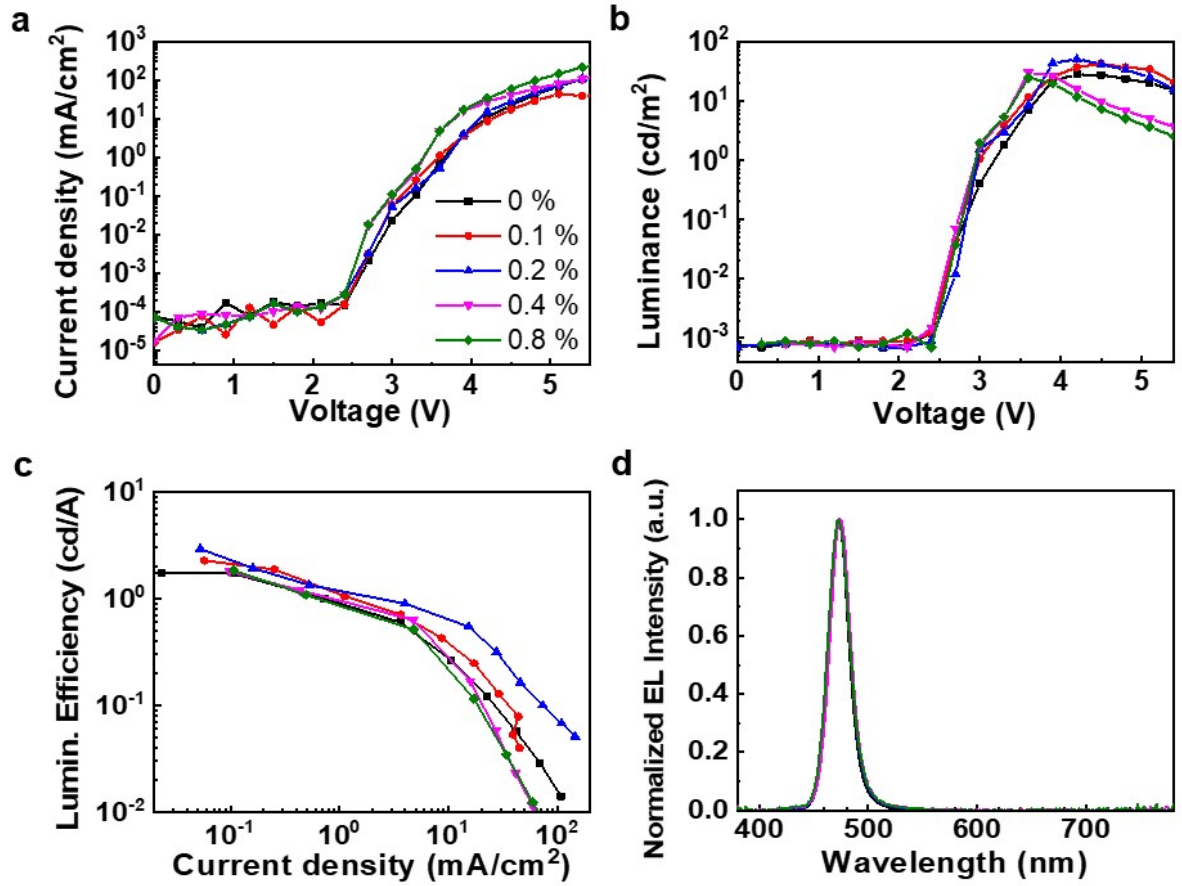

Figure S17. a) Current density–voltage, b) Luminance–voltage, c) Luminous efficiency–current density. d) Normalized electroluminescence spectrum of each PeLED device with different Cd contents.

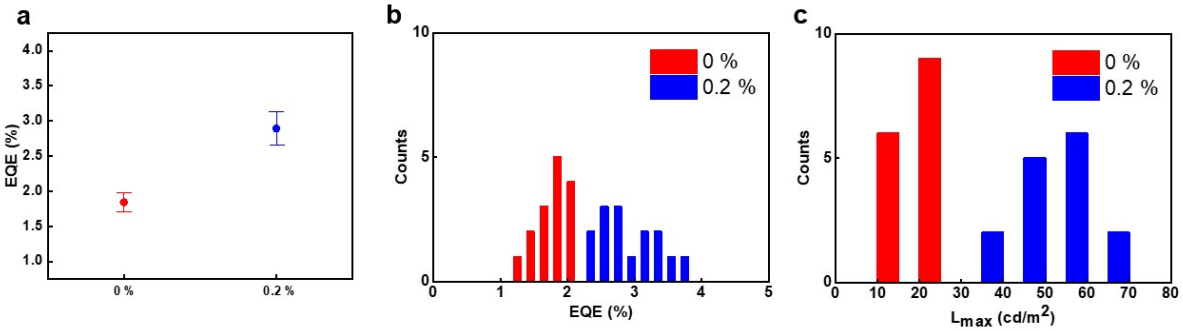

Figure S18. a) Comparison of EQE values for the devices between the 0% and 0.2% Cd content. Histogram of b) maximum EQE and c) maximum luminance of 0 % and 0.2 % Cd content LED devices, measured from 15 devices.

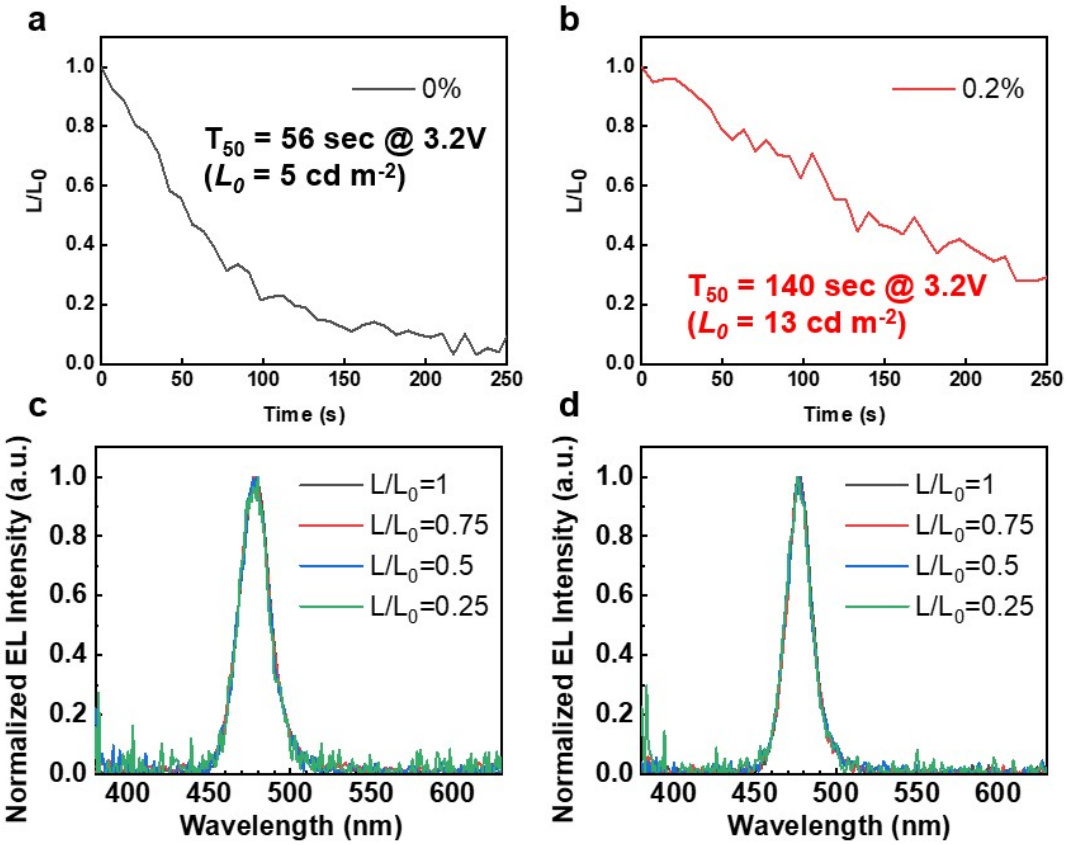

Figure S19. Device stability test from lifetime measurements (T_{50}) of a) 0% and b) 0.2% device at a constant voltage of 3.2V. c-d) Electroluminescence spectra of each step.

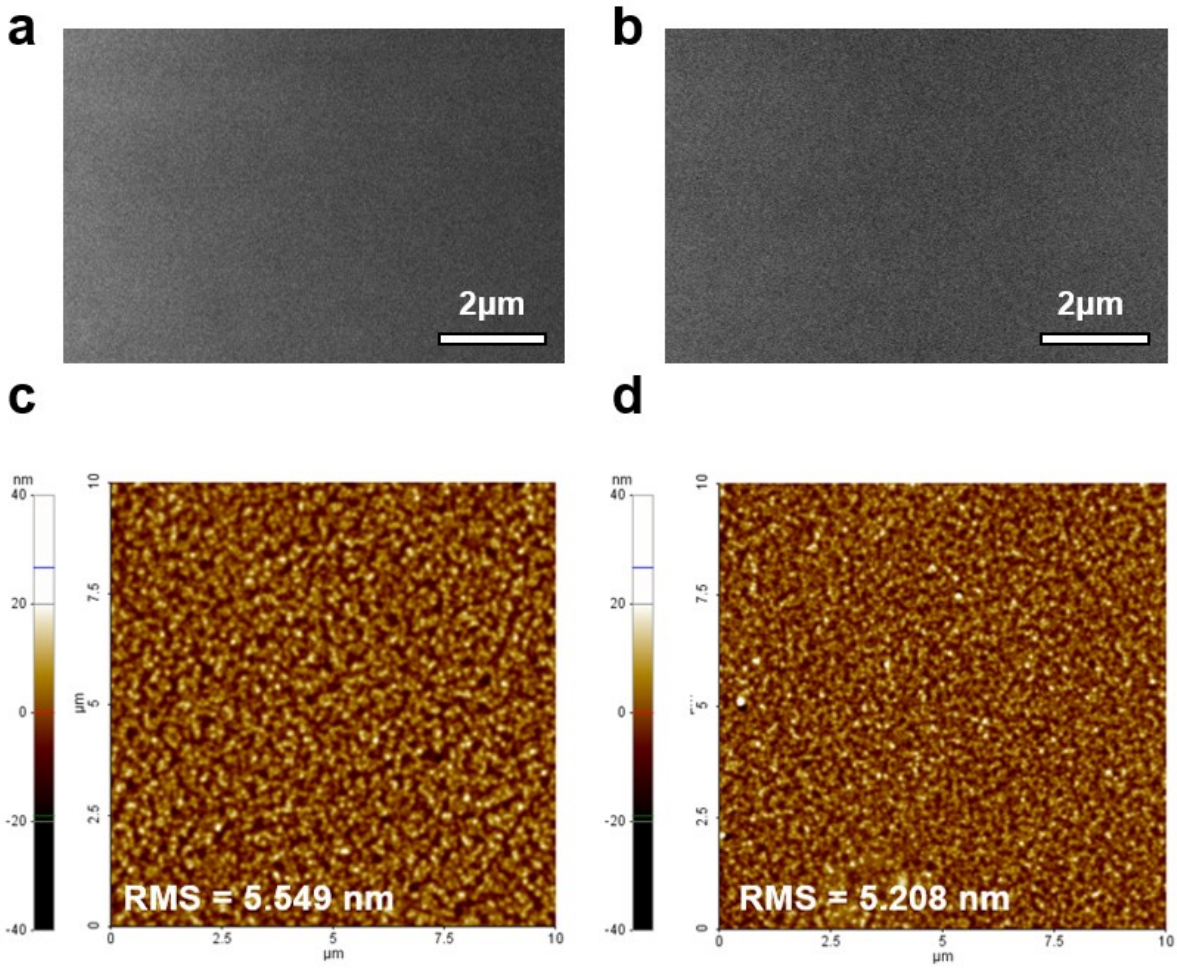

Figure S20. SEM image of a) 0% and b) 0.2% perovskite film and AFM image of c) 0% and d) 0.2% perovskite film.

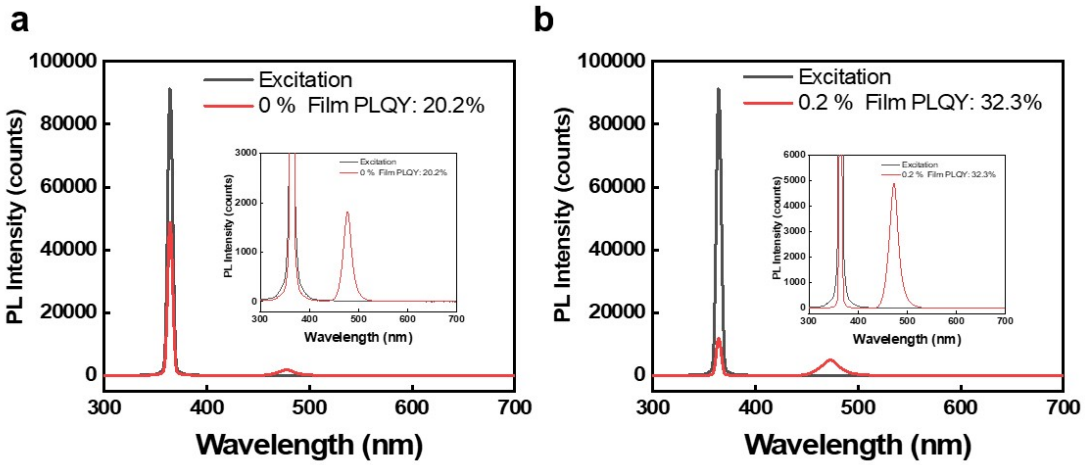

Figure S21. Photoluminescence quantum yield (PLQY) spectra of 0% and 0.2% perovskite film.

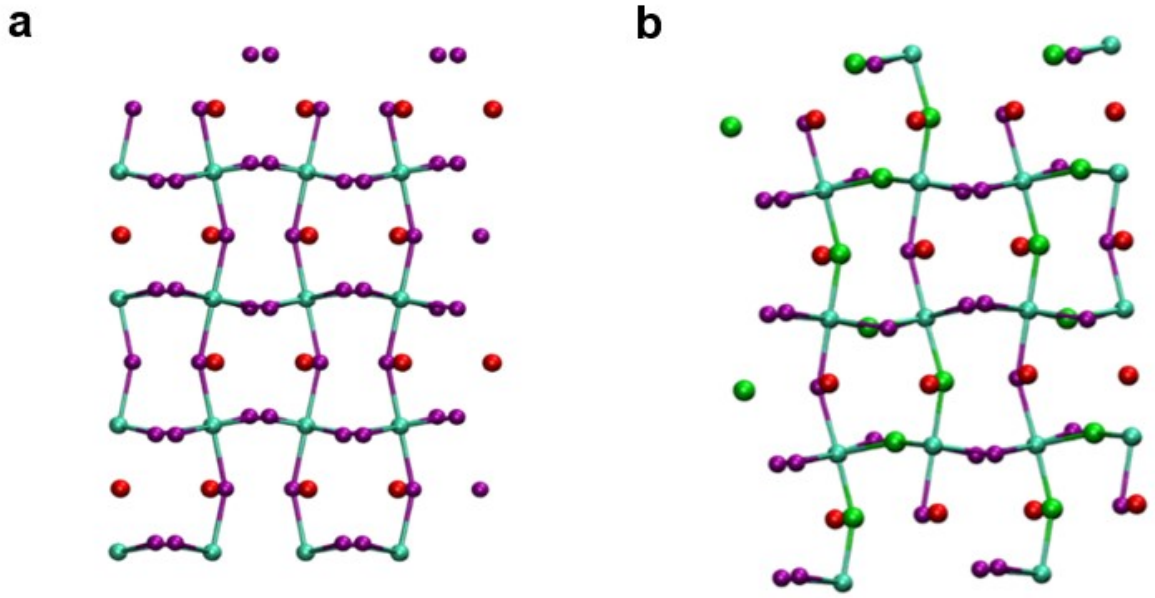

Figure S22. Structural models for bulk a) $CsPbBr_3$ 2×2×2 supercell; b) $CsPbBr_2Cl$ 2×2×2 supercell.

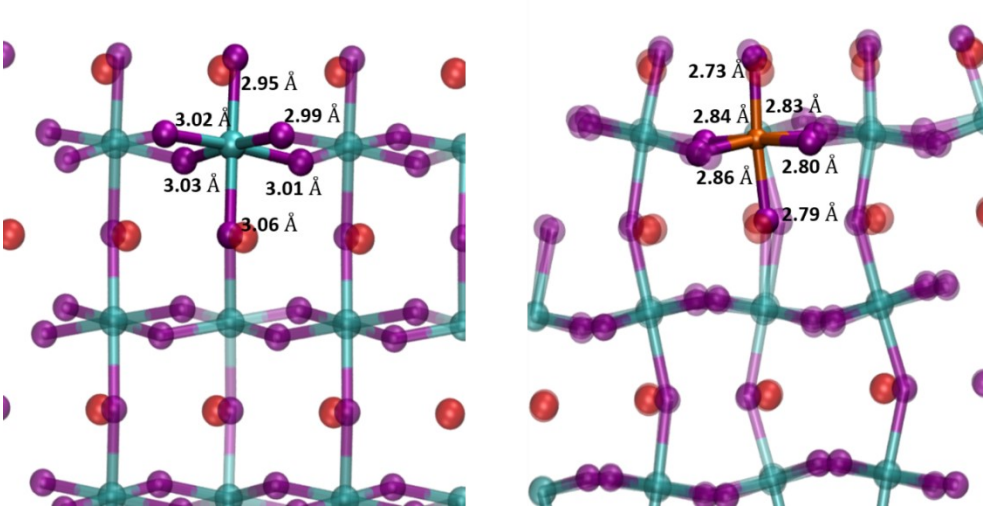

Figure S23. Structure and metal-Br bond lengths in the CsBr-terminated (001) surface of the pristine $CsPbBr_3$ (left) and the same phase with Cd substituting Pb at the surface (right).

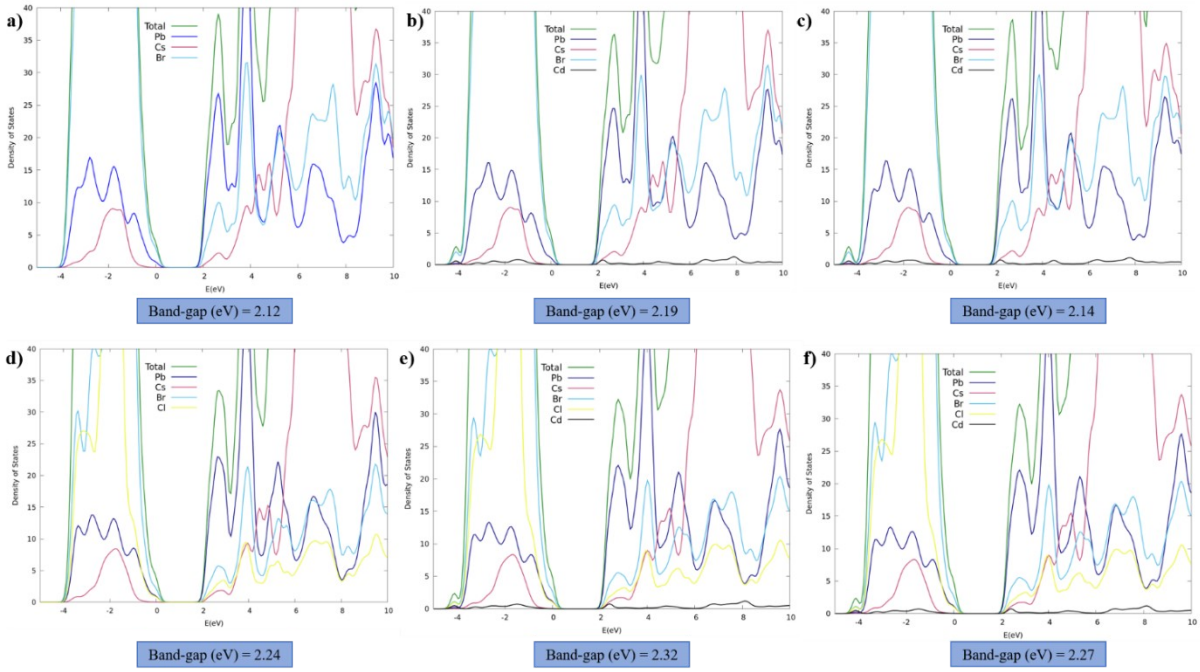

Figure S24. Projected density of states (PDOS) on atomic orbitals of the CsBr-terminated surfaces of pristine and Cd-doped $CsPbBr_3$ and $CsPbBr_2Cl$: a) pristine $CsPbBr_3$; b) Cd substituting lead in the bulk of the $CsPbBr_3$ slab; c) Cd substituting lead at the surface of the $CsPbBr_3$ slab; d) pristine $CsPbBr_2Cl$; e) Cd substituting lead in the bulk of the $CsPbBr_2Cl$ slab; f) Cd substituting lead at the surface of the $CsPbBr_2Cl$ slab.

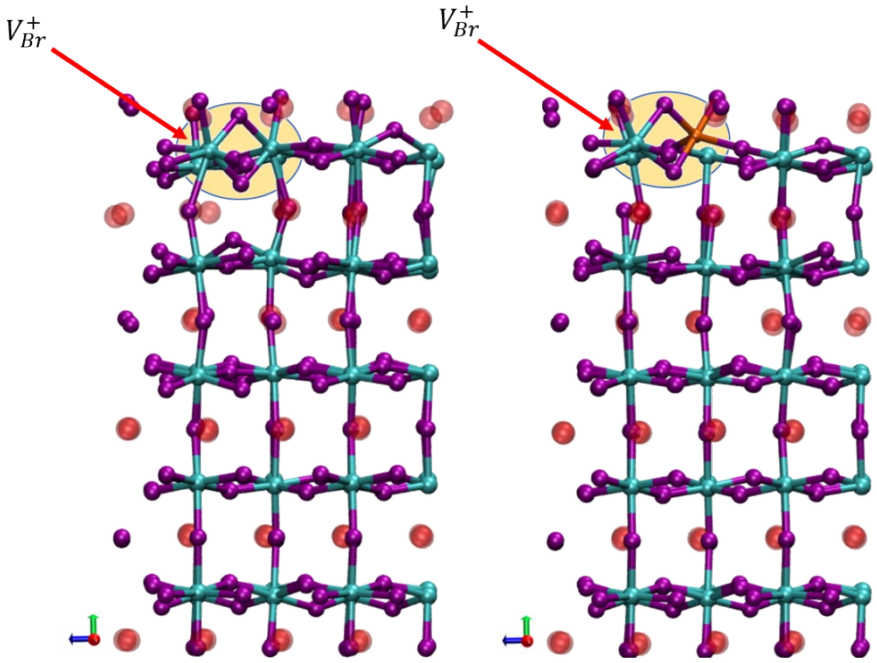

Figure S25. Optimized structures of the Br-Frenkel couple in a) pristine $CsPbBr_3$ and b) Cd_{Pb}-$CsPbBr_3$ slabs

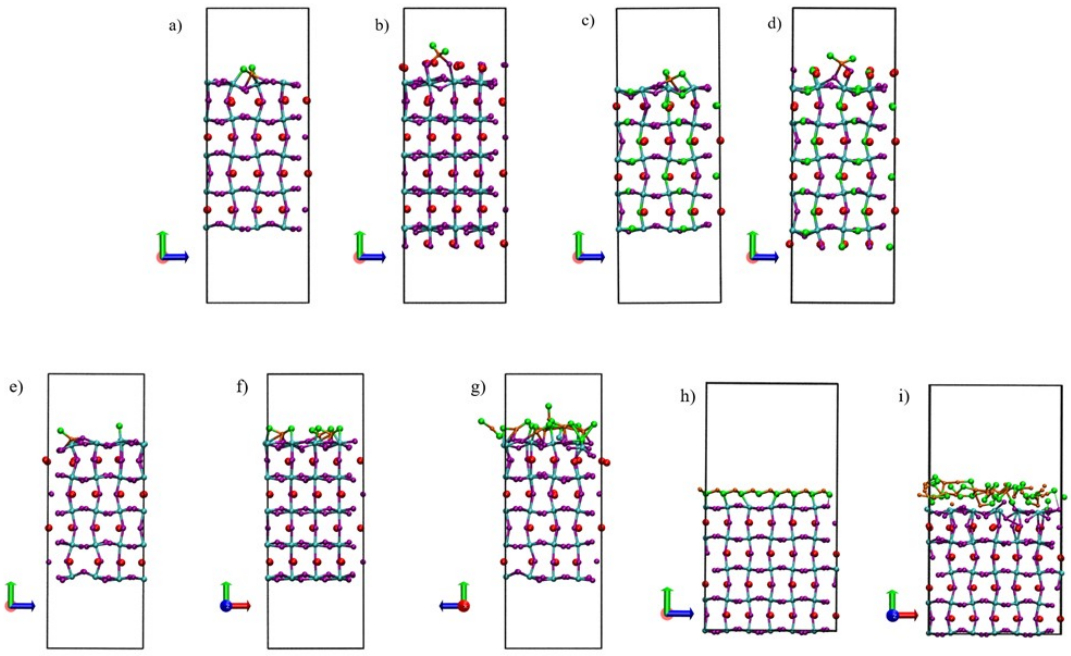

Figure S26. Optimized structures of the (001) surfaces of a) $CsPbBr_3$-PbBr-$CdCl_2$ b) $CsPbBr_3$-CsBr-$CdCl_2$, c) $CsPbBr_2Cl$-PbBr(Cl)-$CdCl_2$ d) $CsPbBr_2Cl$-CsBr(Cl)-$CdCl_2$, e) $CsPbBr_3$-PbBr-$CdCl^+Cl^-$ f) $CsPbBr_3$-PbBr-$CdCl_2$-50% g) $CsPbBr_3$-PbBr-$CdCl_2$-100%, h) $CsPbBr_3$-PbBr-$CdCl_2$-(phase)-initial, i) $CsPbBr_3$-PbBr-$CdCl_2$-(phase)-optimized.

Table S1. Inductively coupled plasma mass analysis of Cd-PNCs actual molar ratios of Pb to Cd.

Sample designation	Nominal molar ratio in precursor solution (PbX_2 : $CdCl_2$)	Actual molar ratio in PNCs (Pb : Cd)
0.1%	0.975 : 0.025	0.999 : 0.001
0.2%	0.950 : 0.050	0.998 : 0.002
0.4%	0.900 : 0.100	0.996 : 0.004
0.8%	0.800 : 0.200	0.992 : 0.008

Table S2. Inductively coupled plasma mass analysis of Cd bulk and surface doping PNCs actual molar ratios of Pb to Cd.

Sample designation	**Actual molar ratio in PNCs (Pb : Cd)**
Cd-Bulk doping (15.2%)	0.848 : 0.152
Cd-Surface doping (1.6%)	0.984 : 0.016

Table S3. Estimated lattice parameters of the PNCs based on PXRD results

Sample	Assigned peak (*hkl*)	Peak position (2*θ*, degree)	Calculated lattice constant (Å)	Average lattice constant (Å)
Non-doped	100	15.46	5.726	5.754
	111	21.79	5.761	
	200	30.95	5.774	
Cd-Surface (0.1%)	100	15.46	5.726	5.755
	111	21.78	5.765	
	200	30.95	5.774	
Cd-Surface (0.2%)	100	15.46	5.726	5.753
	111	21.81	5.756	
	200	30.95	5.774	
Cd-Surface (0.4%)	100	15.46	5.726	5.754
	111	21.78	5.765	
	200	30.97	5.770	
Cd-Surface (0.8%)	100	15.46	5.726	5.754
	111	21.77	5.768	
	200	30.98	5.768	
Cd-Bulk (15.2%)	111	15.42	5.739	5.723
	111	21.99	5.712	
	200	31.26	5.718	

Table S4. Summary of Cd $3d_{5/2}$ peak deconvolution of Cd-PNCs.

Species		Cd@Surface		Cd@Bulk	
		Peak center (eV)	FWHM (eV)	Peak center (eV)	FWHM (eV)
Cd-bulk (15.2%)	As-prepared	404.61	1.05	405.55	1.13
		65.78%		34.22%	
	After surface etching	404.32	1.17	405.42	1.17
		19.29%		80.71%	
Cd-surface (1.6%)	As-prepared	404.45	1.02	405.30	1.02
		80.71%		19.29%	
	After surface etching	-	-	-	-
		-		-	

Table S5. Summary of Cl 2p peak deconvolution of Cd-PNCs.

Species		Cl@Surface		Cl@Bulk	
		Peak center (eV)	FWHM (eV)	Peak center (eV)	FWHM (eV)
Cd-bulk (15.2%)	As-prepared	197.85 199.35	1.34 1.28	197.02 198.65	1.17 1.26
		18.85%		81.15%	
	After surface etching	-	-	197.13 198.77	1.26 1.05
		-		100.00%	
Cd-surface (1.6%)	As-prepared	197.60 199.23	1.14 1.21	196.90 198.53	1.18 1.20
		19.96%		80.04%	
	After surface etching	-	-	196.93 198.58	1.01 0.96
		-		100.00%	

Table S6. Time-resolved PL decay profiles of perovskite NCs solution capped with OLA and OA ligands.

Sample configuration	τ_1 (ns)	A_1 (%)	τ_2 (ns)	A_2 (%)	τ_3 (ns)	A_3 (%)	τ_{avg} (ns)
0%	28.45	3.58	5.34	22.41	0.99	74.01	2.95
0.1%	32.15	4.03	5.88	23.62	0.82	72.35	3.28
0.2%	37.62	3.72	6.84	22.18	1.24	74.10	3.84
0.4%	37.54	2.99	5.81	19.47	0.91	77.54	2.96
0.8%	32.29	3.22	5.21	20.62	0.92	76.15	2.82

τ_1, τ_2, and τ_3: Lifetimes A_1, A_2 and A_3: Respective fractional contributions

τ_{avg}: Average lifetime (τ_{avg}) which is calculated using $\tau_{avg} = \sum_{i=1}^{3} Ai \cdot \tau i$

Table S7. Time-resolved PL decay profiles of perovskite NCs solution capped with DDAB ligand.

Sample configuration	τ_1 (ns)	A_1 (%)	τ_2 (ns)	A_2 (%)	τ_3 (ns)	A_3 (%)	τ_{avg} (ns)
0%	96.84	12.32	28.59	33.35	0.96	54.14	22.04
0.1%	103.85	12.42	33.48	39.43	0.89	48.15	26.53
0.2%	97.25	16.56	28.91	48.97	1.71	34.47	30.85
0.4%	105.87	13.31	29.79	41.91	1.75	44.78	27.26
0.8%	95.53	17.70	28.23	36.08	1.87	46.62	27.97

τ_1, τ_2, and τ_3: Lifetimes A_1, A_2 and A_3: Respective fractional contributions

τ_{avg}: Average lifetime (τ_{avg}) which is calculated using $\tau_{avg} = \sum_{i=1}^{3} Ai \cdot \tau i$

Table S8. Summarized device performances of PeLEDs.[a]

Sample configuration	L_{max} [cd/m^2] @ bias	LE_{max} [cd/A] @ bias	Turn-on Voltage [V] @ 1cd/m^2	Wavelength [nm]
0 %	27.75@4.2	1.73@3.0	3.0	474
0.1 %	42.26@4.5	2.26@3.0	3.0	474
0.2 %	50.55@4.2	2.91@3.0	3.0	475
0.4 %	29.85@3.9	1.79@3.0	3.0	475
0.8 %	24.40@3.6	1.83@3.0	3.0	474

[a]Full device : ITO/PEDOT:PSS/poly-TPD/perovskite NCs/TPBi/LiF/Al

Table S9. Calculated values of work function for $CsPbBr_{3-x}Cl_x$ perovskite slab models with Cd^{2+} incorporation. As previously found, surface termination (or coverage) has a strong impact on the perovskite work function (WF). PbBr-terminated show the highest WF (5.9 eV), CsBr-terminated show the lowest WF (4.6 eV).

System	Nature of doping	WF (eV)
	CsBr terminated	
	Neat	4.62
$CsPbBr_3$	Cd bulk doped	4.69
	Cd surface doped	4.70
	Neat	4.69
$CsPbBr_2Cl$	Cd bulk doped	4.81
	Cd surface doped	4.74
	PbBr terminated	
	Neat	5.96
$CsPbBr_3$	Cd bulk doped	5.99
	Cd surface doped	5.95
	Neat	5.93
$CsPbBr_2Cl$	Cd bulk doped	5.96
	Cd surface doped	5.96

Table S10. Calculated adsorption energy (E_{ads}), band gap (E_{gap}) and work function (WF) of the differently terminated $CsPbBr_3$ and $CsPbBr_2Cl$ slabs. E_{ads} are calculated starting from the CdCl2 bulk phase and molecule.

	E_{ads} (eV) $CdCl_2$ molecule	E_{ads} (eV) $CdCl_2$ Phase	E_{gap} (eV)	WF (eV)
$CsPbBr_3$-CsBr-ter-$CdCl_2$	-1.56	0.18	2.15	4.98
$CsPbBr_3$-PbBr-ter-$CdCl_2$	-1.62	0.11	2.24	6.04
$CsPbBr_3$-PbBr-ter-$CdCl^+$-Cl^-	-1.41	0.34	2.25	6.12
$CsPbBr_3$-PbBr-ter-$CdCl_2$ (50%)	-1.62	0.12	2.23	6.58
$CsPbBr_3$-PbBr-ter-$CdCl_2$ (100%)	-1.48	0.27	2.21	6.35
$CsPbBr_3$-PbBr-ter-$CdCl_2$ (100%-$CdCl_2$ -layer)	/	-0.25 *	/	/
$CsPbBr_2Cl$-CsBr-ter-$CdCl_2$	-1.42	0.32	2.20	5.11
$CsPbBr_2Cl$-PbBr-ter-$CdCl_2$	-1.56	0.19	2.35	6.00

* energy of adsorption calculated starting by the optimized layer of $CdCl_2$ as reported in Figure S26 h-i.

Table S11. Summary of blue (~ 480 nm) emissive perovskite NCs LED performance parameters in the literature.

Perovskite		Emission peak [nm]	EQE [%]	PLQY [%]	L_{max} [cd/m^2]	Reference
Single halide perovskite	$CsPbBr_3$	~480	12.3	~100[a]	~500	*Nat. Nanotechnol.* **2020** 15, 668-674
	$CsPbBr_3$	470	4.7	65[b]	3850	*Adv. Mater.* **2021** 33, 2006722.
	$CsPbBr_3$	465	0.8	40[b]	631	*ACS Energy Lett.* **2021** 2, 477-484
Mixed halide perovskite	$CsPbBr_xCl_{3-x}$	479	0.86	62.3[a]	29.95	*ACS Appl. Mater. Interfaces* **2019** 11, 23401−23409
	$CsPb(Br/Cl)_3$ (K^+-passivation)	477	1.96	38.4[a]	86.95	*Adv. Funct. Mater.* **2020** 1908760
	$CsPb(Br_{1-x}Cl_x)_3$	476	2.25	32[a]	678	*ACS Energy Lett.* **2019** 4, 2703−2711
	$CsPb(Br_xCl_{1-x})_3$	471	6.3	~100[a]	465	*ACS Energy Lett.* **2020** 5, 793−798
	$CsPbCl_{0.99}Br_{2.01}$ (Ni^+-doping)	470	2.4	89[a]	612	*ACS Appl. Mater. Interfaces* **2020** 12, 14195−14202
	$CsPb(Br/Cl)_3$	470	1	50~60[a]	318	*ACS Appl. Mater. Interfaces* **2019** 11, 21655−21660
	$CsPbBr_xCl_{3-x}$	470	0.44	60[a]	11.96	*ACS Appl. Mater. Interfaces* **2019** 11, 23401−23409
	$CsPbBr_xCl_{3-x}$	469	0.5	9[b]	111	*Adv. Mater.* **2018** 30, 1706226
	$(Cs_{0.8}Rb_{0.2})(Pb_{0.95}Ni_{0.05})(Br_{1.8}Cl_{1.2})$	467	2.14	86.7[a]	100~	*Adv. Optical Mater.* **2020** 2001494
	$CsPbBr_xCl_{3-x}$ (Mn^{2+}-doping)	466	2.12	28[a]	245	*Joule* **2018** 2, 11, 2421−2433
	$CsPbCl_{3-x}Br_x$ (TBPO-passivation)	463	3.3	71[a]	569	*Science Bulletin* **2020** 65, 1150−1153
	$CsPb(Br/Cl)_3$	456	1.1	31.8[b]	43.2	*Adv. Optical Mater.* **2020** 2000289
	$CsPbBr_2Cl$ (Cd^{2+}-passivation)	475	3.71	66.8[a]	50.55	**Our work**

a : solution PLQY
b : film PLQY

References

1 T. D. Kühne, M. Iannuzzi, M. D. Ben, V. V. Rybkin, P. Seewald, F. Stein, T. Laino, R. Z. Khaliullin, O. Schutt, F. Schiffmann, D. Golze, J. Wilhelm, S. Chulkov, M. H. Bani-Hashemian, V. Weber, U. Borstnik, M. Taillefumier, A. S. Jakobovits, A. Lazzaro, H. Pabsk, T. Muller, R. Schade, M. Guidon, S. Andermatt, N. Holmberg, G. K. Schenter, A. Hehn, A. Bussy, F. Belleflamme, G. Tabacchi, A. Glob, M. Lass, I. Bethune, C. J. Mundy, C. Plessl, M. Watkins, J. VandeVondele, M. Krack, J. Hutter, *J. Chem. Phys.*, 2020, **152**, 194103.

2 J. P. Perdew, K. Bruke, Y. Wang, *Phys. Rev. B*, 1996, **54**, 16533-16539,

3 S. Grimme, S. Ehrlich, L. Goerigk, *J. Comput. Chem.*, 2011, **32**, 1456-1465,

4 S. Goedecker M. Teter, J. Hutter, *Physical Review B*, 1996, **54**, 1703-1710.

5 J. VandeVondele, J. Hutter, *J. Chem. Phys.*, 2007, **127**, 114105,

6 Y. R. Park, H. H. Kim, S. Eom, W. K. Choi, H. Choi, B. R. Lee, Y. Kang, *J. Mater. Chem. C*, 2021, **9**, 3608-3619.

7 M. Imran, J. Ramede, F. Di Stasio, M. De Franco, J. Buha, S. V. Aert, L. Goldoni, S. Lauciello, M. Prato, I. Infante, S. Bals, L. Manna, *Chem. Mater.*, 2020, **32**, 10641–10652.

8 J. Y. Woo, Y. Kim, J. Bae, T. G. Kim, J. W. Kim, D. C. Lee, S. Jeong, *Chem. Mater.*, 2017, **29**, 7088-7092.